NUMERICAL JUSTIFICATION OF BRANCHED LAMINATED MICROSTRUCTURE WITH SURFACE ENERGY*

ZHIPING LI†

Abstract. A mathematical model is given to study the branched laminated microstructure in austenite-martensite phase transition. A numerical method based on a mesh transformation method is applied to a two dimensional elastic crystal model, and the numerical results show that, for sufficiently small surface energy density and sufficiently long laminates, the branched laminates are energetically favorable, the numerical results also show that there is certain finite order asymptotically self-similar structure in the branched laminates.

Key words. non-quasiconvex energy, branched laminated microstructure, surface energy, self-similarity, mesh transformation method

AMS subject classifications. 73C50,65K10,65N30

1. Introduction. It is well known that many elastic crystals undergo austenitic-martensitic phase transitions across the transformation temperature, when a higher symmetric phase (austenite) above the transformation temperature transforms to a lower symmetric phase (martensite), which often consists of fine mixtures of variants and exhibits finely twined laminated microstructure, below the transformation temperature, and vice versa. It is also observed that the twin laminates can have branched structure and narrow into needles when they approach the austenite-martensite interface.

Mathematical models and analysis based on the energy minimization have been developed to study the equilibrium state of phase transformations and microstructures [1]-[4]. It is believed that the branched structure and the length scale of the microstructure, that is the lengths of the branches and the width of the twinning laminates, are related to the total length of the laminates and the surface energy density on the interfaces between the twins (see [1, 5, 6] among many others). Mathematical analysis on some simplified model problems, by estimating global lower bounds and investigating the local character of energy minimizers, indicates that the branched laminated microstructure with surface energy may be asymptotically self-similar [5, 6]. In fact, with a more detailed study Sergio Conti proved that for the limiting model of Kohn and Müller the branched laminated microstructure is indeed asymptotically self-similar [7]. The phenomenon has also been studied on some one dimensional models [8, 9], where some distinct states or local minima are identified by minimizing the energy subject to a constraint on the geometry or number of "phase trasitions". On the other hand, numerical simulations of branched laminated microstructures on physically nonlinear thermoelastic models have also been studied by using finite element

* This work was supported by the Special Funds for Major State Basic Research Projects (G1999032800), and RFDP of China.
†LMAM, School of Mathematical Sciences, Peking University, Beijing 100871, P.R.China (zpli@math.pku.edu.cn)

approximations on fixed finite element grid [10]. However, since the numerical surface energy, introduced by the incompatibility between the branched laminated structure and the fixed finite element mesh, is often unreasonably large and uncontrolled [11, 12] and there are too many local minima which we do not know any efficient scheme for finding or classifying them, it is difficult, if not impossible, to get reasonably accurate information on the branched laminated microstructures by numerical computations on fixed finite element grid.

In the present paper, a mathematical model for studying the branched structure and the scale of twinned laminated needle-like microstructures is established. The model is based upon minimizing the total potential energy which is considered to be the sum of the elastic energy of the branches and the needles near the austenite-finely-twinned-martensite interface and the surface energy on the sharp interfaces between the martensite variants. In our model, the average elastic energy densities, *i.e.* the average elastic energies per volume, of the branches and the needles are considered to be functions of the twin width and the lengths of the branches and needles, which are established numerically by applying the mesh transformation method (see [13, 14, 15, 16, 17, 18]) to the specially designed boundary value problems to modelling the branched laminated structure and the needle-like microstructures near the austenite-finely-twinned-martensite interface.

The idea of applying the mesh transformation method in our numerical model is to involve the mesh distribution into the minimization procedure so that the mesh can align with the branching and bending twin boundaries and essentially avoid the mesh dependence of the finite element approximation [13, 19, 20, 21, 22] and thus minimize the artificial surface energy introduced by the finite element discretization. Furthermore, the application of the mesh transformation method makes it possible for us to get numerical results with reasonable precision on relatively coarse meshes [14, 15, 16, 17]. In fact, the application of the mesh transformation method is essential for our purpose, since the elastic energy of the twin laminates is sensitive to the shape, especially to the normal direction, of the bending interfaces of the branches and needles and a fixed mesh can hardly reflect such subtle branching and bending structure that we are trying to compute.

Briefly speaking, in the present paper, the branched laminated microstructures with surface energy for a two dimensional Ericksen-James type model are studied by considering "branched" test functions of the type similar to those used in [5, 6, 7] but optimizing their local structure numerically using the mesh transformation method, a special version of finite element method that avoids artificial surface energy [13, 14, 15, 16, 17, 18]. The numerical results confirms that for the physical model the energetically favorable twin laminated microstructure does have an asymptotically self-similar branched structure.

The rest of the paper is arranged as follows. In section 2, a 2-dimensional mathematical model for elastic crystals, which we use in our numerical experiments in the present paper, is presented. In section 3, a mathematical model for branched laminated needle-like microstructures with surface energy is given. In section 4, the mesh transformation method is described. In section 5, numerical examples are presented, and the numerical results show that certain finite order asymptotically self-similar branched structure is indeed energetically favorable to the simple needle-like laminates, provided that the surface energy density is sufficiently small and the total length of the twin laminates is sufficiently large. In section 6, we briefly summarize our main results.

2. A mathematical model for elastic crystals. For the static problem of austenitic-martensitic phase transitions, the well known geometrically nonlinear theory [1, 2] leads to the consideration of minimizing an integral functional

$$F(u;\,\Omega) = \int_\Omega f(\nabla u(x),\ \theta(x))\,dx \tag{2.1}$$

in a set of admissible functions

$$\boldsymbol{U}(u_0;\,\Omega) = \{u \in W^{1,p}(\Omega; R^m) : u = u_0, \text{ on } \partial\Omega_0\}, \tag{2.2}$$

where $\Omega \subset R^n$ is a bounded open set with a Lipschitz continuous boundary $\partial\Omega$, $\partial\Omega_0$ is a subset of $\partial\Omega$ with a positive $(n-1)$-dimensional measure, θ is a given temperature field and $n < p < \infty$, and where the Ericksen-James elastic energy density $f(\cdot,\ \theta)$ is such that $f(\cdot,\ \theta)$ has a unique potential well above the transformation temperature $(\theta > \theta_T)$ and has several symmetry related potential wells below the transformation temperature $(\theta < \theta_T)$ [1, 2, 23, 24]. In geometrically nonlinear elasticity theory, the Ericksen-James elastic energy density $f(\cdot,\ \theta)$ is of the form [25, 24]

$$f(\nabla u,\ \theta) = \Phi(C,\ \theta), \tag{2.3}$$

where $C = (\nabla u)^T \nabla u \in \boldsymbol{S}^n = \{A \in R^{n\times n} : A^T = A\}$, which is the set of symmetric matrices in R^n, is the right Cauchy-Green strain tensor.

In the present paper, we consider a two dimensional model $(n = m = 2)$ with

$$\begin{aligned}\Phi(C,\ \theta) = \frac{b(\theta)}{4}(C_{11} - C_{22})^2 - \frac{c(\theta)}{8}(C_{11} - C_{22})^2|C_{11} - C_{22}| \\ + \frac{d(\theta)}{16}(C_{11} - C_{22})^4 + e\,C_{12}^2 + g(\operatorname{tr} C - 2)^2,\end{aligned} \tag{2.4}$$

where

$$b(\theta) = (1 + \alpha \arctan \mu(\theta - \theta_T))d_0\hat{\varepsilon}^2, \tag{2.5}$$

$$c(\theta) = 2(1 + \frac{1+2\gamma}{3}\alpha \arctan \mu(\theta - \theta_T))d_0\hat{\varepsilon}, \tag{2.6}$$

$$d(\theta) = (1 + \gamma\alpha \arctan \mu(\theta - \theta_T))d_0, \tag{2.7}$$

and where $d_0 > 0$, $e > 0$ and $g > 0$ are the elastic moduli, $\hat{\varepsilon}$ is the transformation strain, θ_T is the transformation temperature,

$$\alpha \approx \frac{2}{\pi},\ \ \mu > 0, \text{ and } \gamma < 1 \tag{2.8}$$

are the material constants used to reflect the change of elastic moduli and the energy barriers as the temperature varies.

Let $\Phi(C,\ \theta)$ be given by (2.4). Then the energy density $f(\nabla u,\ \theta)$ defined by (2.3) has the following properties [15, 16]:

(i) a unique potential well $SO(2)$ for $\theta > \theta_T$;

(ii) two symmetry related rotationally invariant potential wells $SO(2)U_0$ and $SO(2)U_1$ for $\theta < \theta_T$,

where $SO(2)$ is the set of all 2×2 rotational matrices, and

$$U_0 = \begin{pmatrix} \sqrt{1-\hat{\varepsilon}} & 0 \\ 0 & \sqrt{1+\hat{\varepsilon}} \end{pmatrix}, \quad U_1 = \begin{pmatrix} \sqrt{1+\hat{\varepsilon}} & 0 \\ 0 & \sqrt{1-\hat{\varepsilon}} \end{pmatrix}. \tag{2.9}$$

Furthermore, U_0 and $R^{\pm}U_1$ are in rank-one connection. More precisely, let $\eta_1 = \sqrt{1-\hat{\varepsilon}}$ and $\eta_2 = \sqrt{1+\hat{\varepsilon}}$ and let

$$R^{\pm} = \begin{pmatrix} \eta_1\eta_2 & \pm\hat{\varepsilon} \\ \mp\hat{\varepsilon} & \eta_1\eta_2 \end{pmatrix}, \tag{2.10}$$

then, we have

$$R^{\pm}U_1 = U_0 + \mathbf{a}^{\pm} \otimes \mathbf{n}^{\pm}, \tag{2.11}$$

where $\mathbf{a}^{\pm} = \sqrt{2}\hat{\varepsilon}(\eta_1,\ \mp\eta_2)^T$ and $\mathbf{n}^{\pm} = \frac{1}{\sqrt{2}}(1,\ \pm 1)^T$.

While the energy minimizing sequences take a crucial role in the computation of Young measures which give the probability distribution of the microstructure, the local minimizers of the energy $F(u;\ \Omega)$ in $\mathbf{U}(u_0;\ \Omega)$ can also be of great importance, especially in the case, as is in this paper, when profiles of the branches and the needles play a crucial role. In fact, it is such local minimizers, which contain the detailed information of the branches and the needles, that we are trying to model and compute in this paper.

3. A mathematical model for branched needles. Near the transformation temperature ($\theta = \theta_T$), the martensitic and austenitic phases may coexist, and in such a case the martensitic twins are observed to branch and narrow into needles as they approach the austenite-twinned-martensite interface. It is believed in some theories that the length scale of the branches and the width of the twinned laminates are determined by the balance of the elastic energy, which is introduced by the narrowing of the twins, and the surface energy, which is defined on the interfaces of the twins [1, 2, 5, 6]. In the following, we are going to derive a computational model for this approach.

Without loss of generality, we may assume that the gradients of the martensitic twins are U_0 and R^-U_1, the volume fractions are $(1-\lambda)$ and λ respectively, and thus the average of deformation gradients is $A_\lambda^- = (1-\lambda)U_0 + \lambda R^- U_1$. Let

$$\xi^{\pm} = \arctan\frac{\lambda\hat{\varepsilon}(\eta_1+\eta_2)}{(1+\lambda\hat{\varepsilon})\eta_1 + (1-\lambda\hat{\varepsilon})\eta_2} \pm \arctan\frac{\hat{\varepsilon}\sqrt{1+4\lambda(\lambda-1)}}{1+\eta_1\eta_2}, \tag{3.1}$$

$$\varphi^{\pm} = \arctan \frac{(1-\lambda\hat{\varepsilon})\eta_2 - \cos\xi^{\pm}}{\lambda\hat{\varepsilon}\eta_2 - \sin\xi^{\pm}}, \tag{3.2}$$

where $\hat{\varepsilon}$ is the transformation strain and $\eta_1 = \sqrt{1-\hat{\varepsilon}}$, $\eta_2 = \sqrt{1+\hat{\varepsilon}}$ (see section 2). Then, it is easily verified that A_λ^- is rank-one connected to the austenitic potential well $SO(2)$ at exactly two rotational matrices

$$R(\xi^{\pm}) = \begin{pmatrix} \cos\xi^{\pm} & -\sin\xi^{\pm} \\ \sin\xi^{\pm} & \cos\xi^{\pm} \end{pmatrix},$$

and for some vectors $\mathbf{b}^{\pm} \in R^2$,

$$A_\lambda^- - R(\xi^{\pm}) = \mathbf{b}^{\pm} \otimes \mathbf{n}(\varphi^{\pm}), \tag{3.3}$$

where $\mathbf{n}(\varphi) = (\cos\varphi,\ \sin\varphi)^T$. Therefore, the austenite-twinned-martensite interface has to be normal to either $\mathbf{n}(\varphi^+)$ or $\mathbf{n}(\varphi^-)$. Noticing that $\mathbf{n}^- = \mathbf{n}(-\pi/4)$, we see that the periodic relationship

$$u\Big(x + \frac{w\,\mathbf{n}(\varphi^{\pm}+\pi/2)}{\cos(\pi/4-\varphi^{\pm})}\Big) - A_\lambda^-\Big(x + \frac{w\,\mathbf{n}(\varphi^{\pm}+\pi/2)}{\cos(\pi/4-\varphi^{\pm})}\Big) = u(x) - A_\lambda^-(x), \quad \forall x \in R^2$$

holds for both the deformation of the twinned martensite with the twin width w and the deformation of the austenite $R(\xi^{\pm})x$. This periodicity allows us to consider a periodic problem on a parallelogram with one pair of parallel sides, of which the length is the multiple of $\frac{w\,\mathbf{n}(\varphi^{\pm}+\pi/2)}{\cos(\pi/4-\varphi^{\pm})}$, perpendicular to $\mathbf{n}(\varphi^{\pm})$ and the other pair of parallel sides perpendicular to $\mathbf{n}^-$.

Now, we consider a pair of twin laminate which branches k times before narrowing into needles near the austenite-martensite interface as is shown in figure 3.1 where $k=3$, and we consider the total elastic energy of such a structure as a function of the twin width w, the branches lengths L_b^i, $i = 1, 2, \ldots, k$, the needle length L_n, and the total laminate length $L = L_0 + L_n/2 + \sum_{i=1}^k L_b^i$, which can be obtained by computing the elastic energy of the needles and each of the branches.

Let Ω be a parallelogram centered at 0 with the length of the sides perpendicular to $\mathbf{n}^-$ being l. Let the boundary conditions u_n be given by

$$u_n(x) = \begin{cases} u_n\big(x \mp \dfrac{w\,\mathbf{n}(\varphi^-+\pi/2)}{\cos(\pi/4-\varphi^-)}\big), & \text{on } \partial\Omega^{\pm}, \\ U_0\,(x - w(\frac{1}{2}-\lambda)\mathbf{n}^-) + (\int_0^{w^{-1}x\cdot\mathbf{n}^-} \tau_\lambda(s)\,ds)\mathbf{a}^-, & \text{on } \partial\Omega_-, \\ R(\xi^-)(x - w(\frac{1}{2}-\lambda)\mathbf{n}^-), & \text{on } \partial\Omega_+ \end{cases} \tag{3.4}$$

and the boundary conditions u_b be given by

$$u_b(x) = \begin{cases} u_b\big(x \mp \dfrac{w\,\mathbf{n}(\varphi^-+\pi/2)}{\cos(\pi/4-\varphi^-)}\big), & \text{on } \partial\Omega^{\pm}, \\ U_0\,(x - w(\frac{1}{2}-\lambda)\mathbf{n}^-) + (\int_0^{w^{-1}x\cdot\mathbf{n}^-} \tau_\lambda(s)\,ds)\mathbf{a}^-, & \text{on } \partial\Omega_-, \\ U_0\,(x - \frac{w}{3}(\frac{1}{2}-\lambda)\mathbf{n}^-) + (\int_0^{3w^{-1}x\cdot\mathbf{n}^-} \tau_\lambda(s)\,ds)\mathbf{a}^-, & \text{on } \partial\Omega_+, \end{cases} \tag{3.5}$$

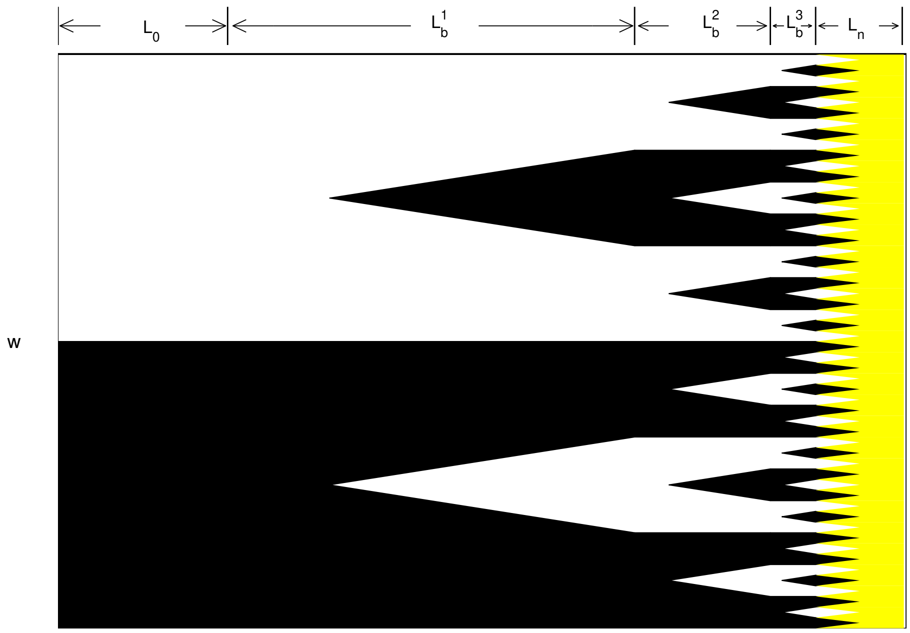

FIG. 3.1. *The geometry of the branched needle-like microstructure.*

where $\partial\Omega^{\pm}$ are the pair of sides perpendicular to $\mathbf{n}^-$, $\partial\Omega_{\pm}$ are the pair of sides perpendicular to $\mathbf{n}(\varphi^-)$, and

$$\tau_\lambda(s) = \begin{cases} 0, & k-\lambda \le s - \frac{1}{2} < k, \qquad \forall k \in \mathcal{I}, \\ 1, & k-1 \le s - \frac{1}{2} < k-\lambda, \ \forall k \in \mathcal{I}, \end{cases}$$

where $\mathcal{I}$ is the set of all integers. It is easily seen [1, 21] that u_n defines a pair of twin laminate on $\partial\Omega_-$ and an austenite on $\partial\Omega_+$, and that u_b defines a pair of twin laminate on $\partial\Omega_-$ and three pairs of twin laminates on $\partial\Omega_+$(see figure 3.2).

The domain Ω is said to have an admissible decomposition for needles, if Ω can be divided into three disjoint connected subdomains Ω_i, $i = 0, 1, 2$ with Lipschitz continuous boundaries $\partial\Omega^i = \partial\Omega_i \setminus \partial\Omega_-$, $i = 1, 2$, each of which consists of two single valued monotone curves as shown in figure 3.2. Let the set of admissible functions $U_n(u_n;\,\Omega) \subset U(u_n;\,\Omega)$ be the set of all functions $u \in U(u_n;\,\Omega)$ such that the sets

$$\Omega^0 = \{x \in \Omega : |\nabla u(x) - R(\xi^-)| < |\nabla u(x) - U_0| \wedge |\nabla u(x) - R^- U_1|\},$$
$$\Omega^1 = \{x \in \Omega : |\nabla u(x) - U_0| < |\nabla u(x) - R^- U_1| \wedge |\nabla u(x) - R(\xi^-)|\},$$
$$\Omega^2 = \{x \in \Omega : |\nabla u(x) - R^- U_1| < |\nabla u(x) - U_0| \wedge |\nabla u(x) - R(\xi^-)|\},$$

where $\alpha \wedge \beta = \min\{\alpha, \beta\}$, give an admissible decomposition of Ω for needles.

The domain Ω is said to have an admissible decomposition for branches, if Ω can be divided into four disjoint connected subdomains, which can be grouped into two

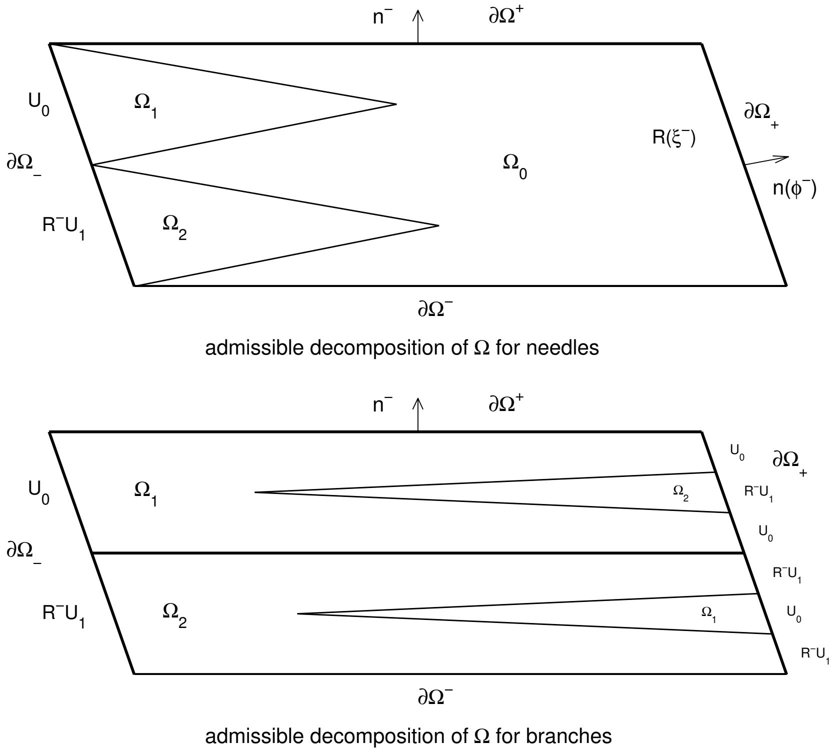

FIG. 3.2. *The geometry of needles and branches.*

sets Ω_1 and Ω_2 as shown in figure 3.2, and the set $\partial\Omega^{1,2} = \partial\Omega_1 \cap \partial\Omega_2$ consists of three disjoint Lipschitz continuous branches $\partial\Omega_0^{1,2}$, $\partial\Omega_1^{1,2}$ and $\partial\Omega_2^{1,2}$, with $\partial\Omega_0^{1,2}$ dividing Ω into lower and upper parts in the middle, and $\partial\Omega_1^{1,2}$, $\partial\Omega_2^{1,2}$, each of which consists of two single valued monotone curves, being in the lower and upper parts respectively. Let the set of admissible functions $U_b(u_b;\ \Omega) \subset U(u_b;\ \Omega)$ be the set of all functions $u \in U(u_b;\ \Omega)$ such that the sets

$$\Omega^1 = \{x \in \Omega : |\nabla u(x) - U_0| < |\nabla u(x) - R^- U_1|\},$$
$$\Omega^2 = \{x \in \Omega : |\nabla u(x) - R^- U_1| < |\nabla u(x) - U_0|\},$$

give an admissible decomposition of Ω for branches.

For the elastic energy of needles, we consider the problem

$$\begin{cases} \text{find } u \in U_n(u_n;\ \Omega) \text{ such that} \\ F(u;\ \Omega) = \inf_{v \in U_n(u_n;\ \Omega)} F(v;\ \Omega). \end{cases} \tag{3.6}$$

Basically, the problem (3.6) is to find the energy minimizer among all possible needles. Denote the elastic energy of a twin needles $u \in U_n(u_n;\ \Omega)$ by $E_n(l, w, u)$, and define the elastic energy of the minimizing twin needles by

$$E_n(l, w) = \inf_{u \in U_n(u_n;\ \Omega)} E_n(l, w, u). \tag{3.7}$$

We have, by scaling $u_\delta(x) = \delta\, u(\delta^{-1}x)$, that

$$E_n(\delta\, l,\ \delta\, w) = \delta^2 E_n(l,\ w). \tag{3.8}$$

Denote $S_n(l, w, u)$ the total interface length of the two needles $(\cup_{i=1}^2 \partial\Omega^i) \setminus \partial\Omega_-$. Let $\{u^{(\alpha)}\} \subset U_n(u_n;\ \Omega)$ be minimizing sequences of problem (3.6), define

$$S_n(l, w) = \inf_{\{u^{(\alpha)}\}} \liminf_{\alpha\to\infty} S_n(l, w, u^{(\alpha)}). \tag{3.9}$$

It is easily seen, by scaling, that

$$S_n(\delta\, l, \delta\, w) = \delta S_n(l, w), \tag{3.10}$$

Similarly, for the elastic energy of branches, we consider the problem

$$\begin{cases} \text{find } u \in U_b(u_b;\ \Omega) \text{ such that} \\ F(u;\ \Omega) = \inf_{v\in U_b(u_b;\ \Omega)} F(v;\ \Omega). \end{cases} \tag{3.11}$$

Likewise, the problem (3.11) is to find the energy minimizer among all admissible branches. Denote the elastic energy of an admissible branch $u \in U_b(u_b;\ \Omega)$ by $E_b(l, w, u)$, and define the elastic energy of the minimizing branch by

$$E_b(l, w) = \inf_{u\in U_n(u_n;\ \Omega)} E_b(l, w, u). \tag{3.12}$$

We have, by scaling $u_\delta(x) = \delta\, u(\delta^{-1}x)$, that

$$E_b(\delta\, l,\ \delta\, w) = \delta^2 E_b(l,\ w). \tag{3.13}$$

Denote $S_b(l, w, u)$ the total interface length of the admissible branched laminate ($2l+$ length of $\partial\Omega^{1,2}$). Let $\{u^{(\alpha)}\} \subset U_b(u_b;\ \Omega)$ be minimizing sequences of problem (3.11), define

$$S_b(l, w) = \inf_{\{u^{(\alpha)}\}} \liminf_{\alpha\to\infty} S_b(l, w, u^{(\alpha)}). \tag{3.14}$$

It is easily seen, by scaling, that

$$S_b(\delta\, l, \delta w) = \delta S_b(l, w), \tag{3.15}$$

Let $\Omega_{n,\infty}$ be a infinite domain obtained by the periodic extension of Ω in the direction of $\mathbf{n}(\varphi^- \pm \pi/2)$, and let $U_n(u_n;\ \Omega_{n,\infty})$ be the set of periodic extensions to $\Omega_{n,\infty}$ of all functions in $U_n(u_n;\ \Omega)$. It is not difficult to see that for functions in $U_n(u_n;\ \Omega_{n,\infty})$ there are, in average, w^{-1} twins on the left hand side boundary of $\Omega_{n,\infty}$ with respect to per unit width in $\mathbf{n}^-$ direction.

Now, we consider a laminated needle-like microstructure with k orders of branches as follows: Let Ω_∞ be a infinite domain similar to $\Omega_{n,\infty}$. On the right hand side of

Ω_∞ it is a twin needles structure introduced by $U_n(u_n;\ \Omega_{n,\infty})$ with twin width $3^{-k}w$ and the length of the domain $\Omega_{n,\infty}$ in the direction perpendicular to $\mathbf{n}^-$ being L_n, attached sequentially to the left are the branched laminated twin structure with twin width $3^{i-k+1}w$ and length L_b^{k-i} for $i = 0, 1, \ldots, k-1$ followed by a simple laminated twin structure with twin width w and length L_0 (see figure 3.1). Typically, the total length of a twin microstructure, measured from the left hand side boundary of Ω_∞ to the needle tip, is

$$L = L_0 + L_n/2 + \sum_{i=1}^{k} L_b^i. \tag{3.16}$$

Define the characteristic length of the needles $\hat{L}_n$ and the characteristic length of the i's branch $\hat{L}_b^i$ by

$$\hat{L}_n = L_n\, 3^k w^{-1}, \tag{3.17}$$

$$\hat{L}_b^i = L_b^i\, 3^{i-1} w^{-1}, \quad \text{for } i = 1, \ldots, k. \tag{3.18}$$

Let $E(L, \hat{L}_b^1, \ldots, \hat{L}_b^k, \hat{L}_n; w)$ be the average total potential energy of such a microstructure on per unit width of Ω_∞ in $\mathbf{n}^-$ direction. We have, by summing up the surface energy and the elastic energy of the needles, and by using (3.8), (3.10), (3.13) and (3.15), that

$$\begin{aligned} &E^k(L, \hat{L}_b^1, \ldots, \hat{L}_b^k, \hat{L}_n; w) \\ &= 2\, L\, \sigma_s\, w^{-1} + w\, \Big(\sum_{i=1}^{k} 3^{1-i}\, E_b(\hat{L}_b^i, 1) + 3^{-k}\, E_n(\hat{L}_n, 1)\Big) \\ &\quad + \sigma_s\, \Big(\sum_{i}^{k} (S_b(\hat{L}_b^i, 1) - 3^{1-i}\, 2\, \hat{L}_b^i) + S_n(\hat{L}_n, 1) - 3^{-k}\, \hat{L}_n\Big), \end{aligned} \tag{3.19}$$

where σ_s is the surface energy density which is assumed to be an elastic constant defined on twin boundaries as well as on needle boundaries.

For a given specimen with total twin microstructure length L, the energetically preferred branched twin laminated needle-like microstructure is given by the solution of the following problem

$$\begin{cases} \text{find } k \geq 0,\ w > 0 \text{ and } (\hat{L}_n, \hat{L}_b^1, \ldots, \hat{L}_b^k) \in \boldsymbol{L}(L, w, k), \text{ such that} \\ E^k(L, \hat{L}_b^1, \ldots, \hat{L}_b^k, \hat{L}_n; w) = \displaystyle\inf_{\substack{m \geq 0,\ \tilde{w} > 0, \\ (\tilde{L}_n, \tilde{L}_b^1, \ldots, \tilde{L}_b^m) \in \boldsymbol{L}(L, \tilde{w}, m)}} E^m(L, \tilde{L}_b^1, \ldots, \tilde{L}_b^m, \tilde{L}_n; \tilde{w}), \\ \end{cases} \tag{3.20}$$

where

$$\begin{aligned} \boldsymbol{L}(L, w, k) = \{(\hat{L}_n, \hat{L}_b^1, \ldots, \hat{L}_b^k) :\ & \hat{L}_n, \hat{L}_b^1, \ldots, \hat{L}_b^k > 0, \\ & \text{and } w\, (3^{-k} \hat{L}_n + \sum_{i=1}^{k} 3^{1-i} \hat{L}_b^i) \leq L\}. \end{aligned} \tag{3.21}$$

LEMMA 3.1. *Suppose that* $(k, w, \hat{L}_n, \hat{L}_b^1, \ldots, \hat{L}_b^k)$ *is a solution of problem* (3.20) *satisfying*

$$w\,(3^{-k}\hat{L}_n + \sum_{i=1}^{k} 3^{1-i}\hat{L}_b^i) < L,$$

then $\hat{L}_n, \hat{L}_b^1, \ldots, \hat{L}_b^k$ *are the minimizers of the functions*

$$g_n^k(l) = E_n(l,1) + \frac{\sigma_s}{w}(3^k S_n(l,1) - l), \tag{3.22}$$

$$g_b^i(l) = E_b(l,1) + \frac{\sigma_s}{w}(3^{i-1} S_b(l,1) - 2l), \quad i = 1, \ldots, k, \tag{3.23}$$

respectively. Suppose further that the functions $E_b(\cdot,1)$, $E_n(\cdot,1)$, $S_b(\cdot,1)$ *and* $S_n(\cdot,1)$ *are differentiable, then we have*

$$w = \Big(\frac{2\,L\,\sigma_s}{\sum_{i=1}^k 3^{1-i} E_b(\hat{L}_b^i,1) + 3^{-k}E_n(\hat{L}_n,1)}\Big)^{\frac{1}{2}}, \tag{3.24}$$

$$\frac{\partial E_n}{\partial \hat{L}_n}(\hat{L}_n,1) = \frac{\sigma_s}{w}\,(1 - 3^k \frac{\partial S_n}{\partial \hat{L}_n}(\hat{L}_n,1)). \tag{3.25}$$

$$\frac{\partial E_b}{\partial \hat{L}_b^i}(\hat{L}_b^i,1) = \frac{\sigma_s}{w}\,(2 - 3^{i-1} \frac{\partial S_b}{\partial \hat{L}_b^i}(\hat{L}_b^i,1)), \tag{3.26}$$

Proof. Since $(\hat{L}_n, \hat{L}_b^1, \ldots, \hat{L}_b^k)$ minimizes the functional $E^k(L, \hat{L}_b^1, \ldots, \hat{L}_b^k, \hat{L}_n; w)$, by (3.19), $\hat{L}_n, \hat{L}_b^1, \ldots, \hat{L}_b^k$ must minimizes $g_n^k(l)$, $g_b^i(l)$, for $i = 1, \ldots, k$ simultaneously. The equations (3.24)-(3.26) follows from

$$\frac{\partial E^k}{\partial w} = \frac{\partial E^k}{\partial \hat{L}_n} = \frac{\partial E^k}{\partial \hat{L}_b^i} = 0, \quad i = 1, \ldots, k.$$

□

LEMMA 3.2. *Let* $g_n^k(l)$, $g_b^i(l)$, $i = 1, \ldots, k$ *be defined by* (3.22) *and* (3.23). *Suppose that* $E_b(\cdot,1)$, $E_n(\cdot,1)$, $S_b(\cdot,1)$ *and* $S_n(\cdot,1)$ *are differentiable and satisfy*

$$\lim_{l\to 0} E_b(l,1) = \lim_{l\to 0} E_n(l,1) = +\infty, \tag{3.27}$$

$$\lim_{l\to\infty}(S_b(l,1) - 2l) = \lim_{l\to\infty}(S_n(l,1) - l) = +\infty, \tag{3.28}$$

Then, for any given $w > 0$, *the problem*

$$\begin{cases} \text{find } \hat{L}_n(w) > 0,\ \hat{L}_b^i(w) > 0,\ i = 1, \ldots, k \text{ such that} \\ g_n^k(l),\ g_b^i(l),\ i = 1, \ldots, k \text{ are minimized} \end{cases} \tag{3.29}$$

has a solution which satisfy the equations (3.25) *and* (3.26).

Proof. The conclusion of the lemma is obvious. □

REMARK 3.1. *We do not really need the* ∞ *in the conditions* (3.27) *and* (3.28), *it can be replaced by a sufficiently large number. It is in such a sense that the conditions* (3.27) *and* (3.28) *are justified by numerical experiments.*

Let σ_s be fixed. For a given $w > 0$, denote the solution of the problem (3.29) by $\hat{L}_n(w) > 0$, $\hat{L}_b^i(w) > 0$, $i = 1, \ldots, k$. Define

$$E^k(L, w) = E^k(L, \hat{L}_b^1(w), \ldots, \hat{L}_b^k(w), \hat{L}_n(w); w). \tag{3.30}$$

For given $L > 0$ and $\sigma_s > 0$, consider the problem

$$\begin{cases} \text{find } k \geq 0,\ w > 0 \text{ such that} \\ E^k(L, w) = \inf\limits_{m \geq 0,\ \tilde{w} > 0} E^m(L, \tilde{w}). \end{cases} \tag{3.31}$$

THEOREM 3.1. *Let* $L > 0$ *and* $\sigma_s > 0$ *be given. Suppose that* (k, w) *is a solution of the problem* (3.31), *and* $(\hat{L}_n(w) > 0,\ \hat{L}_b^i(w) > 0,\ i = 1, \ldots, k)$ *is a solution of the problem* (3.29) *such that the inequality*

$$w\,(3^{-k}\hat{L}_n(w) + \sum_{i=1}^{k} 3^{1-i}\hat{L}_b^i(w)) \leq L \tag{3.32}$$

holds. Then, $(k, w, \hat{L}_n(w), \hat{L}_b^1(w), \ldots, \hat{L}_b^k(w))$ *is a solution of the problem* (3.20).

Proof. Since (k, w) is a solution of the problem (3.31), by the definition of $\hat{L}_n(w)$, $\hat{L}_b^1(w), \ldots, \hat{L}_b^k(w)$, we have

$$E^k(L, \hat{L}_b^1(w), \ldots, \hat{L}_b^k(w), \hat{L}_n(w); w) \leq E^k(L, \tilde{L}_b^1, \ldots, \tilde{L}_b^m, \tilde{L}_n; \tilde{w}),$$
$$\forall m \geq 0, \tilde{w}, \tilde{L}_b^1, \ldots, \tilde{L}_b^m, \tilde{L}_n > 0. \tag{3.33}$$

The theorem follows as a consequence of the inequalities (3.32) and (3.33). ∎

By summarizing the above discussion, we see that, in our model, the computation of the branched needle-like laminated microstructure consists of the following five steps:

Step 1 To establish the functions $E_n(l, 1)$, $E_b(l, 1)$, $S_n(l, 1)$ and $S_b(l, 1)$ by solving the problems (3.6) and (3.11);

Step 2 To establish the function $E^k(L, w)$ for given k and L as a function of w by solving the problem (3.29);

Step 3 To find the minimizer of $E^k(L, w)$ for given k and L;

Step 4 To find the solution of (3.31) by comparing the results obtained in step 3 for various k;

Step 5 To check the validity of the inequality (3.32).

It is clear that the step 1 is the core of the model.

REMARK 3.2. *We do not consider the situation when the inequality* (3.32) *fails to hold, since our numerical experiments show that the inequality* (3.32) *is always satisfied by the solutions of the problems* (3.31) *and* (3.29).

4. The mesh transformation method. Consider the problem of minimizing the functional

$$F(u;\ \Omega) = \int_\Omega f(\nabla u(x))\, dx \tag{4.1}$$

on a set of admissible functions

$$\boldsymbol{U}(u_0; \Omega) = \{u \in W^{1,p}(\Omega; R^m) : u(x) = u_0(x),\ \text{on } \partial\Omega_0\}. \tag{4.2}$$

In our application, the domain Ω is taken to be a parallelogram with sides of length $2a$ and $2b$ perpendicular to $\mathbf{n}(\alpha \pm \pi/2)$ and $\mathbf{n}(\beta)$ respectively, where $\mathbf{n}(\tau) = (\cos(\tau), \sin(\tau))^T$. More precisely, $\Omega = r_0(\alpha,\beta)\,\hat{\Omega}$ where $\hat{\Omega} = (-a,\ a) \times (-b,\ b)$ is a $2a \times 2b$ rectangular domain, $r_0(\alpha,\beta)$ is defined by

$$r_0(\alpha,\beta)\begin{pmatrix} x \\ y \end{pmatrix} = R(\alpha)\begin{pmatrix} x + y\tan(\alpha-\beta) \\ y \end{pmatrix}, \tag{4.3}$$

and

$$R(\alpha) = \begin{pmatrix} \cos\alpha & -\sin\alpha \\ \sin\alpha & \cos\alpha \end{pmatrix} \tag{4.4}$$

is a rotational matrix.

Assume that the angles α and β are so chosen that the laminated microstructure is periodically defined on Ω along the direction $\mathbf{n}(\beta \pm \pi/2)$ [15, 10], and thus the problem is equivalent to compute, on a domain which is infinite in the directions $\pm r_0(\alpha,\beta)(0,b)^T$, a solution which is periodic in the $\mathbf{n}(\beta \pm \pi/2)$ with period $2b/\cos(\alpha - \beta)$.

Define

$$\begin{aligned} T(\Omega) = \{&\text{bijections } r : \bar{\Omega} \to \bar{\Omega} | r \in W^{1,\infty}(\Omega;\ R^m), r^{-1} \in W^{1,\infty}(\Omega), \\ &\qquad r(\partial\Omega_0) = \partial\Omega_0,\ \text{and } \det\nabla r > 0, a.e. \text{ in } \Omega\}. \end{aligned}$$

For any $r \in T(\Omega)$ and $u \in \boldsymbol{U}(u_0;\Omega)$, let $A \in R^{mn}$ and let $\bar{u}(x) : \Omega \to R^m$ be defined by

$$\bar{u}(x) = u(r(x)) - A\, r(x). \tag{4.5}$$

Then it is easily seen that $\bar{u} \in \boldsymbol{U}(\bar{u}_0;\Omega)$, where $\bar{u}_0(x) = u_0(r(x)) - A\, r(x)$,

$$\int_\Omega f(A + \nabla\bar{u}(x)(\nabla r(x))^{-1}) \det\nabla r(x)\, dx = F(u;\ \Omega), \tag{4.6}$$

and

$$\inf_{\bar{u}\in\boldsymbol{U}(\bar{u}_0;\Omega)} F(\bar{u}, r;\ \Omega) = \inf_{u\in\boldsymbol{U}(u_0;\Omega)} F(u;\ \Omega), \tag{4.7}$$

where

$$F(\bar{u}, r;\, \Omega) = \int_\Omega f(A + \nabla \bar{u}(x)(\nabla r(x))^{-1}))\det \nabla r(x)\, dx. \tag{4.8}$$

Since the problem is periodically defined in the directions $\mathbf{n}(\beta \pm \pi/2)$ (*i.e.* the directions $\pm r_0(\alpha, \beta)(0, b)^T$), the mesh transformation map r and the deformation $\bar{u}$ are naturally asked to satisfy the periodic condition:

$$(r - I)(r_0(\alpha, \beta)((x, b)^T)) = (r - I)(r_0(\alpha, \beta)((x, -b)^T)), \forall x \in [-a,\, a], \tag{4.9}$$

$$\bar{u}(r_0(\alpha, \beta)(x, b)^T) = \bar{u}(r_0(\alpha, \beta)(x, -b)^T), \quad \forall x \in [-a,\, a], \tag{4.10}$$

where I is the identity map.

Let $\mathcal{T}_h(\Omega)$ be regular triangulations of Ω with mesh size h [26]. Let

$$T_h(\Omega) = \{r \in T(\Omega) : r|_K \text{ is affine } \forall K \in \mathcal{T}_h(\Omega),\ r \text{ satisfies (4.9)}\}, \tag{4.11}$$

$$\boldsymbol{U}_h = \{\bar{u} \in (C(\overline{\Omega}))^m : \bar{u}|_K \text{ is affine } \forall K \in \mathcal{T}_h(\Omega), \text{ and (3.10) is satisfied}\} \tag{4.12}$$

and

$$\boldsymbol{U}_h(v; \Omega) = \{\bar{u} \in \boldsymbol{U}_h : \bar{u}|_{\partial\Omega_0} = v\}. \tag{4.13}$$

Instead of finding a minimizer of $F(u;\, \Omega)$ in a fixed finite element function space $\boldsymbol{U}_h(u_0; \Omega)$, we solve the following discrete problem :

$$(MTM) \quad \begin{cases} \text{find } (\bar{u}_h,\, r_h) \in \boldsymbol{U}_h(\bar{u}_0;\, \Omega) \times T_h(\Omega) \text{ such that} \\ F(\bar{u}_h, r_h;\, \Omega) = \inf_{(u', r') \in \boldsymbol{U}_h(\bar{u}_0;\, \Omega) \times T_h(\Omega)} F(u', r';\, \Omega), \end{cases} \tag{4.14}$$

and use its solution $(\bar{u}_h,\ r_h)$ and the relation (4.5) to construct a finite element solution

$$u_h(x) = \bar{u}_h(r_h^{-1}(x)) + A\, x. \tag{4.15}$$

This is the so called mesh transformation method (for a more general form and the convergence analysis of the mesh transformation method, see [17, 14]), which by (4.5)-(4.7) is equivalent to minimizing the elastic energy $F(\cdot;\, \Omega)$ among all finite element function spaces introduced by $\mathcal{T}_h(\Omega)$ and $T_h(\Omega)$, and thus is capable of producing much better numerical results than working on a fixed finite element function space.

5. Numerical experiments and results. Let $f(\nabla u;\, \theta)$ be given by (2.3) and (2.4). For a given total twin microstructure length L and a given surface energy density σ_s, to determine the structure of the branched needle-like laminated microstructure, by section 3, we need to know, as the most important thing of all, the functions $E_n(l, 1)$, $S_n(l, 1)$, $E_b(l, 1)$ and $S_b(l, 1)$. To establish the functions numerically, we first solve the problem (3.6) and (3.11) by the mesh transformation method given in section 4 for a set of discrete data $(l,\ w)$, and then fit the numerical results with some properly chosen curves by using the least square method.

Let $\alpha = \frac{\pi}{4}$ and $\beta = \varphi^-$ which is given by (3.2). Let $\Omega = r_0(\alpha,\beta)\hat{\Omega}$, where $\hat{\Omega} = (-a,\ a) \times (-b,\ b)$ is a $2a \times 2b$ rectangular domain and $r_0(\alpha,\beta)$ is defined by (4.3). Let $\mathcal{T}_{N,M}(\Omega) = \mathcal{T}_h(\Omega)$ be a family of regular triangulations defined by

$$\mathcal{T}_{N,M}(\Omega) = \mathcal{T}_h(\Omega) = \mathcal{T}_h(r_0(\alpha,\beta)\hat{\Omega}) = \{r_0(\alpha,\beta)K : \forall K \in \mathcal{T}_h(\hat{\Omega})\}, \tag{5.1}$$

where $\mathcal{T}_h(\hat{\Omega}) = \mathcal{T}_{N,M}(\hat{\Omega})$, for $h = h_{N,M} = \frac{2}{N \cdot M}\sqrt{(aM)^2 + (bN)^2}$ with $N \geq 2$ and $M \geq 2$, is a family of regular triangulations of $\hat{\Omega}$ introduced by the lines

$$\begin{cases} y = & -b + \frac{2b}{M}i, & 0 \leq i \leq M; \\ x = & -a + \frac{2a}{N}j, & 0 \leq j \leq N; \\ y = & \frac{Nb}{Ma}(x+a) + b - \frac{4b}{M}k, & 0 < k < \frac{M+N}{2}; \\ y = & \frac{-Nb}{Ma}(x-a) - b + \frac{4b}{M}k, & 0 < k < \frac{M+N}{2}. \end{cases} \tag{5.2}$$

Let

$$\partial\Omega_{\pm} = \{x \in \partial\Omega : x = r_0(\alpha,\beta)(\pm a, \eta)^T, -b \leq \eta \leq b\} \tag{5.3}$$

and

$$\partial\Omega^{\pm} = \{x \in \partial\Omega : x = r_0(\alpha,\beta)(\xi, \pm b)^T, -a \leq \xi \leq a\}. \tag{5.4}$$

Let the temperature distribution $\theta(x)$ be a linear function given by

$$\theta(x) = \theta(r_0(\alpha,\beta)(\xi,\eta)^T) = \theta_- + \frac{\theta_+ - \theta_-}{2\,a}(\xi + a), \tag{5.5}$$

which takes the value of $\theta_\pm$ on $\partial\Omega_\pm$.

In our numerical experiments, we set the width of the reference configuration $2b = 0.1$, and set the elastic constants $\alpha = 2.02/\pi$, $\mu = 0.25$, $\gamma = 0$, $\hat{\varepsilon} = 0.05$, $d_0 = 500$, $e = 3.5$ and $g = 15$ (see (2.4)-(2.7)). The transformation temperature is taken to be $\theta_T = 70\,^\circ$C. The initial temperature distribution $\theta(x)$ for the needle problem (3.6) is given by (5.5) with $\theta_- = 69.65\,^\circ$C and $\theta_+ = 70.95\,^\circ$C, while the initial temperature distribution $\theta(x)$ for the branch problem (3.11) is $\theta_- = \theta_+ = 55\,^\circ$C. The volume fraction λ is taken to be 0.5.

The initial mesh for the needle problem (3.6) is introduced by taking $M = 4$ and $N = 2$. The initial deformation $u_0(x)$ is introduced in the following way: let the boundary value $u_n(x)$ be given by (3.4) with $w = 2b = 0.1$, let $u_0(x) \in \mathcal{T}_{2,4}(\Omega)$, which is a piecewise linear finite element function defined on a mesh with $M = 4$ and $N = 2$, satisfy $u_0(x) = u_n(x)$ for all $x \in \partial\Omega_\pm$ and $u_0(x) = R(\xi^-)(x - w(\frac{1}{2} - \lambda)\mathbf{n}^-)$ if $\theta(x) \geq \theta_T$.

The initial mesh for the branch problem (3.11) is introduced by taking $M = 12$ and $N = 4$. The initial deformation $u_b(x)$ is introduced in the following way: let the boundary value $u_b(x)$ be given by (3.5) with $w = 2b = 0.1$, let $u_0(x) \in \mathcal{T}_{4,12}(\Omega)$ satisfy

$$u_0(x) = \begin{cases} U_0\,(x - w(\frac{1}{2} - \lambda)\mathbf{n}^-) + (\int_0^{w^{-1}x\cdot\mathbf{n}^-} \tau_\lambda(s)\,ds)\mathbf{a}^-, & \forall x_1 \leq -0.5a, \\ u_0(x) = U_0\,(x - \frac{w}{3}(\frac{1}{2} - \lambda)\mathbf{n}^-) + (\int_0^{3w^{-1}x\cdot\mathbf{n}^-} \tau_\lambda(s)\,ds)\mathbf{a}^-, & \forall x_1 \geq 0. \end{cases}$$

It is easily seen that u_0 defines a pair of twin structure on the left quarter of the domain, and defines three pairs of twin structure on the right half of the domain.

The mesh transformation method described in section 4 is applied to solve the discrete problems of (3.6) and (3.11), and the conjugate gradient method is used to search for the minimizers. To avoid the elements being deformed too much and too fast where the initial deformation gradient is well away from the wells, the mesh transformation map r is kept fixed in the beginning of the minimizing process until the drop of the elastic energy is getting lost of its initial momentum. To guarantee that the condition $\det \nabla r(x) > 0$ is satisfied in the minimization process, it is checked on each element in the linear search along the direction given by the conjugate gradient method and the step length is reduced whenever necessary. When certain convergence criteria (say $\|\nabla F\|_2 < 0.25 \times 10^{-6}$) is satisfied, the search is continued with the mesh being refined by a factor of 4 until the mesh is sufficiently fine. In our numerical experiments, the finest mesh for the needle is set to be $M = 256$ and $N = 128$, and the finest mesh for the branch is set to be $M = 384$ and $N = 128$. Then, the temperature distribution $\theta(x)$ is set to be a uniform distribution at the transformation temperature θ_T, and the minimizer is searched by the conjugate gradient method with the finite element functions $(\bar{u}_{h,\theta}, r_{h,\theta})$ produced by the above computation as the initial data. The numerical results thus obtained is denoted by $(\bar{u}_{h,\theta_T}, r_{h,\theta_T})$. By section 4, the final mesh defined on the material reference configuration Ω is

$$\mathcal{T}_{h,\theta_T}(\Omega) \equiv \mathcal{T}_h(r_{h,\theta_T}\Omega) = \{r_{h,\,\theta_T}K : \forall K \in \mathcal{T}_h(\Omega)\}, \tag{5.6}$$

by (4.11) and by taking $A = A_\lambda^-$, the finite element minimizing deformation is given by

$$u_{h,\theta_T}(x) = \bar{u}_{h,\theta_T}(r_{h,\theta_T}^{-1}(x)) + A_\lambda^- x. \tag{5.7}$$

Some typical profiles of the needles on the deformed configuration for the twin needle width w and various needle lengths l are shown in figure 5.1, where x_1 and y_1 are the length scales corresponding to the directions $\mathbf{n}(\pi/4)$ and $\mathbf{n}(3\pi/4) = \mathbf{n}^-$ respectively, and where an element is painted in white, black or grey if its deformation gradient is closer to U_0, $R^- U_1$ or $R(\xi^-)$ respectively. It is clearly seen that, as the characteristic length of the needles increases, the needles change their shape from strictly concave to partially convex and finally grow into the twin laminate near the flat end of the needles.

The numerical results of $E_n(l, 1)$ and $S_n(l, 1)$ at some discrete points are shown in table 5.1.

Now, we are going to establish the approximate functions of $E_n(l,\ 1)$ and $S_n(l,\ 1)$ by using the discrete numerical results obtained. Since the numerical results show that the value of $E_n(l,\ 1)$ drops quite fast to its limit as l increases, we consider it to be an exponential function of the form

$$E_n(l,\ 1) = E_n(\infty,\ 1) + \exp(c_1 - c_2 l), \tag{5.8}$$

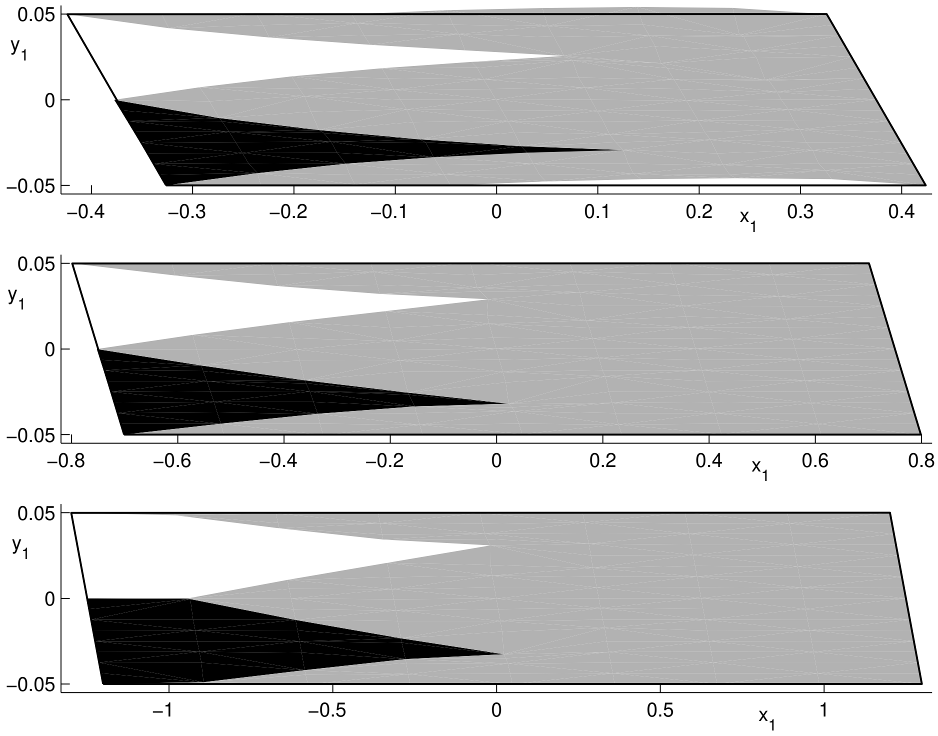

FIG. 5.1. *The needle profiles for $w = 0.1$ and $l = 0.75, 1.5, 2.5$ respectively.*

TABLE 5.1
Some numerical results of $E_n(l, 1)$ and $S_n(l, 1)$.

l	7.5	10.0	12.5	15.0	17.5	20.0
E_n	6.22×10^{-4}	4.14×10^{-4}	3.14×10^{-4}	2.72×10^{-4}	2.43×10^{-4}	2.33×10^{-4}
S_n	17.015	21.375	21.397	23.601	27.875	31.077

where $E_n(\infty, 1) = \lim_{l\to\infty} E_n(l, 1)$, $c_1 \in R^1$ and $c_2 > 0$ are material constants to be determined. By applying the nonlinear least square method to some discrete numerical results of $E_n(l, 1)$, we obtain $E_n(\infty, 1) = 2.243 \times 10^{-4}$, $c_1 = -5.522$ and $c_2 = 0.3075$, of which the l^2-norm of the relative error is 3.5×10^{-2}. For $S_n(l, 1)$, we simply use a cubic spline with not-a-knot boundary condition to fit the discrete numerical results. Figure 5.2 shows the numerical approximations of $E_n(\cdot, 1)$ and $S_n(\cdot, 1)$, where the discrete numerical data used are shown as $*$s.

Having established the numerical approximations of $E_n(\cdot, 1)$ and $S_n(\cdot, 1)$, we turn our attention to establishing the functions $E_b(\cdot, 1)$ and $S_b(\cdot, 1)$. First, we notice that our numerical experiments show that the profiles of the branches for various branch length l_b look essentially the same. The initial data and the numerical result of a typical branch is shown in figure 5.3.

The numerical results of $E_b(l, 1)$ and $S_b(l, 1)$ at some discrete points are shown in

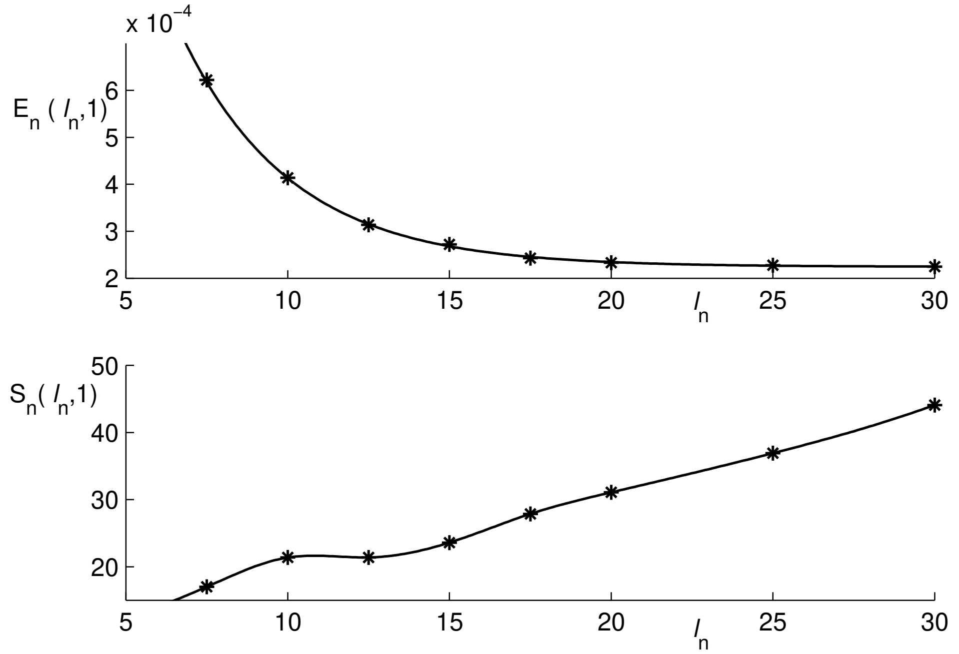

FIG. 5.2. *The numerical approximations of* $E_n(\cdot,\ 1)$ *and* $S_n(\cdot,\ 1)$.

table 5.2.

TABLE 5.2
Some numerical results of $E_b(l,1)$ *and* $S_b(l,1)$.

l	50.0	100.0	150.0	200.0	250.0	300.0
E_b	1.029×10^{-4}	5.070×10^{-5}	3.391×10^{-5}	2.549×10^{-5}	2.031×10^{-5}	1.697×10^{-5}
S_b	250.04562	500.04281	750.04233	1000.0421	1250.0420	1500.0419

By the numerical results, we see that $l \times E_b(l,\ 1)$ are almost a constant for various l, and that the interface of the twin branches consists of nearly straight line segments. So, we assume that the functions $E_b(l,1)$ and $S_b(l,1)$ have the form

$$E_b(l,\ 1) = \delta\, l^{-1}, \tag{5.9}$$

$$S_b(l,\ 1) = \beta_1\, l + \beta_2\,(l+\beta_3)^{-1}. \tag{5.10}$$

By using the least square method, we obtain $\delta = 5.1210639 \times 10^{-3}$, and the l^2-norm of the relative error is 4.8×10^{-2}. For $S_b(\cdot,\ 1)$, we take $\beta_1 = 5$, $\beta_2 = 54^{-1}$ and $\beta_3 = 18^{-1}$, the l^2-norm of the relative error is 1.4×10^{-3}. Figure 5.4 shows the numerical approximation results of the functions $E_b(\cdot,\ 1)$ and $S_b(\cdot,\ 1)$ where the discrete numerical data used are marked by $\times$s.

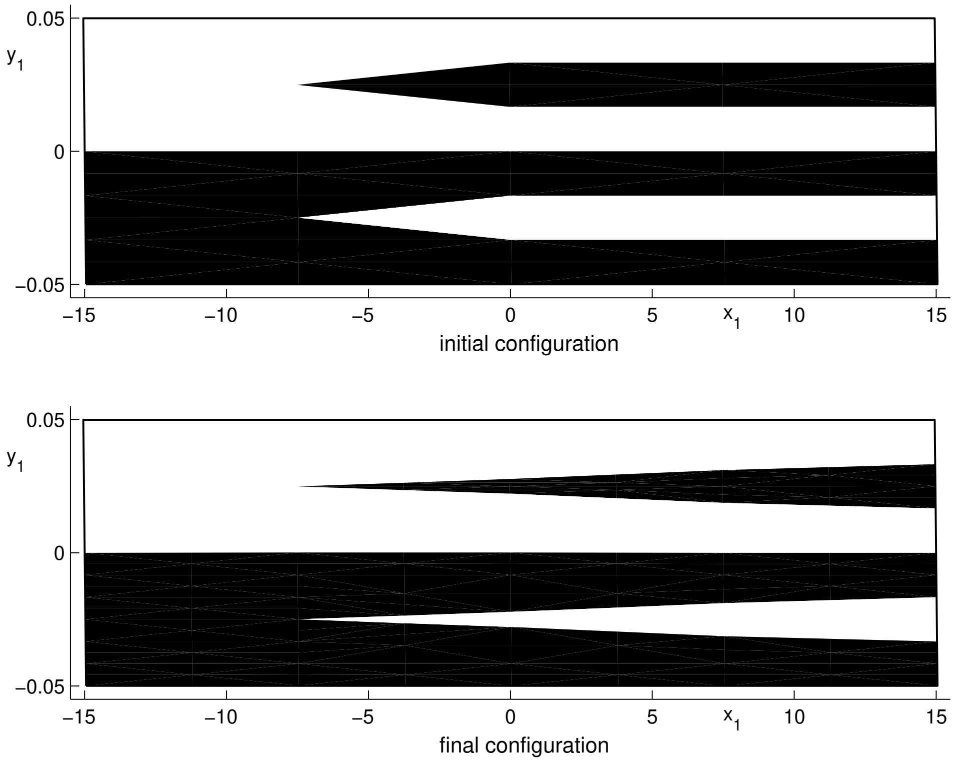

FIG. 5.3. *The profile of a branch: initial and final configurations.*

Using the approximate functions of $E_n(\cdot,1)$, $S_n(\cdot,1)$, $E_b(\cdot,1)$ and $S_b(\cdot,1)$ given above, we can easily establish the functions $E^k(L,w)$ (see (3.30)) for fixed k by applying the golden section search method to solving the problem (3.29). The minimizer of $E^k(L,\cdot)$ for fixed k and L can also be obtained by the golden section search method. The minimizing energy for fixed k and L can then be given by

$$E^k(L) = \inf_{w>0} E^k(L,w) = \inf_{w>0} E^k(L, \hat{L}_b^1(w), \ldots, \hat{L}_b^k(w), \hat{L}_n(w); w). \tag{5.11}$$

By comparing $E^i(L)$ for $i = 0, \ldots,$ and verifying the condition (3.32), we can then find the solution of the problem (3.20).

Some numerical results of comparing $E^i(L)$ with $E^k(L)$ for various branch order $i \le k$ and surface energy density σ_s are shown in figure 5.5. Figure 5.6 shows the relationship between the branched needle length

$$L_s^k(L) = w\,(3^{-k}\hat{L}_n(w) + \sum_{i=1}^{k} 3^{1-i}\hat{L}_b^i(w)), \tag{5.12}$$

which is the sum of the needle length and the lengths of the sequential branches

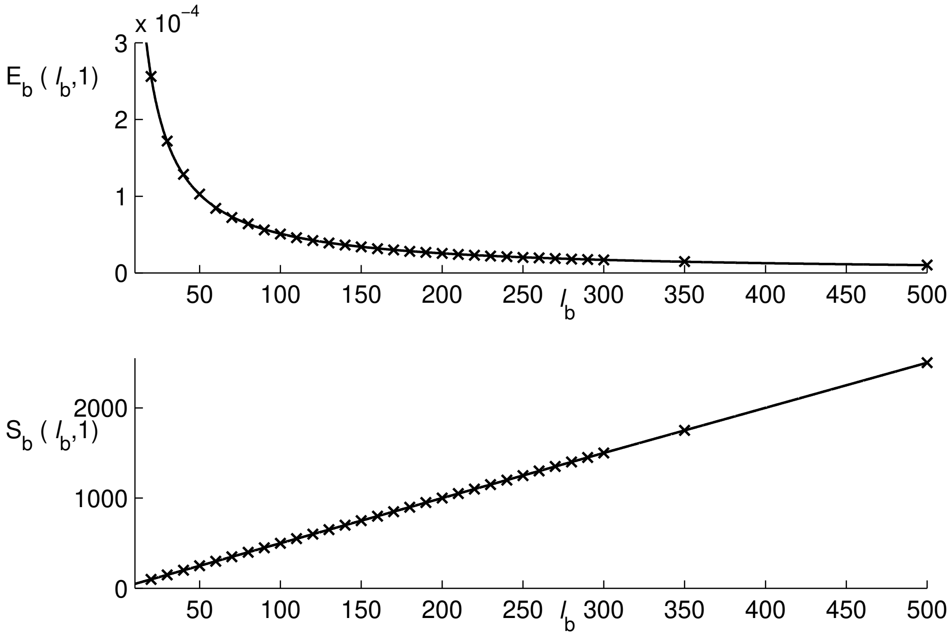

FIG. 5.4. *The numerical approximations of $E_b(\cdot,\,1)$ and $S_b(\cdot,\,1)$.*

from order 1 to k in the branched needle structure, and the total length of the twin microstructure L for $\sigma_s = 10^{-8}$ and $\sigma_s = 10^{-12}$, and it is clearly seen that

$$L_s^k(L) \leq L/3, \quad \forall k. \tag{5.13}$$

This verifies (3.32). In fact, our numerical experiments show that (5.13) holds for all σ_s sufficiently small (say $\leq 10^{-6}$).

Since (3.32) holds, by figure 5.5, we can easily see that for sufficiently large surface energy density and short total laminate length, for example $\sigma_s \geq 10^{-8}$, $L \leq 5$, the needle-like laminated microstructure without branch is energetically favorable, while for sufficiently small surface energy density and long total laminate length, for example $\sigma_s \leq 10^{-10}$, $L \geq 1$, the branched needle-like laminated microstructure is energetically favorable.

Further study of the numerical results reveal some interesting features of the energetically favorable branched laminates.

First, we study the self-similarity of the branches. Table 5.3 shows the numerical results of L_b^i/L_b^{i+1} for the minimizers of the problem (3.20), which turn out to be independent of σ_s and L.

In fact, it follows from (3.26), (5.9) and (5.10) that, for the energy minimizers of the

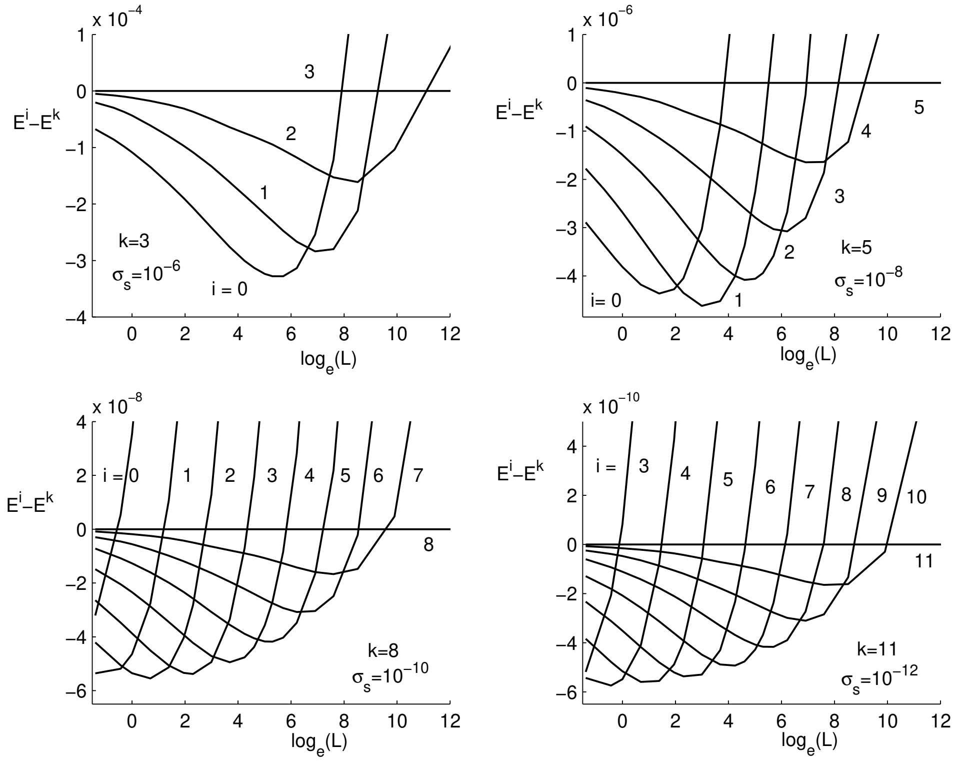

FIG. 5.5. *Difference between $E^i(L)$ and $E^k(L)$ for some k and σ_s.*

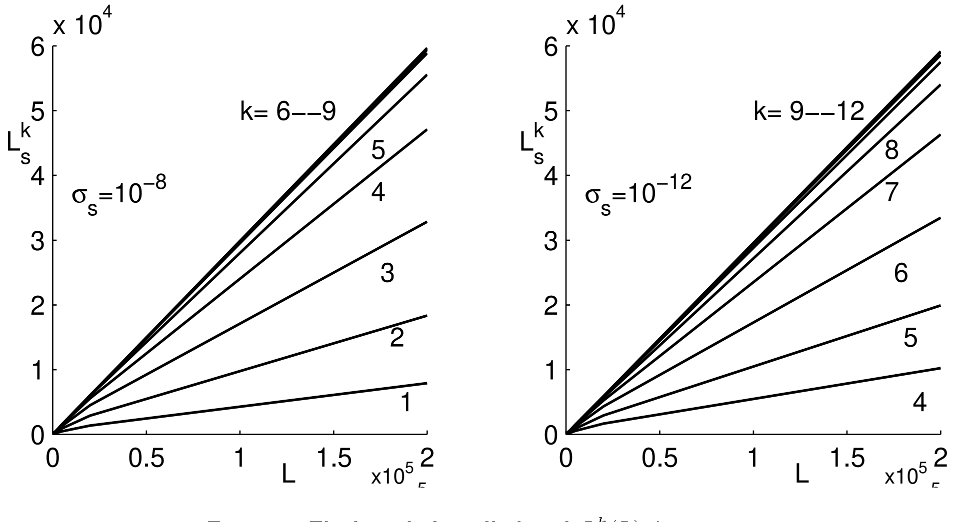

FIG. 5.6. *The branched needle length $L_s^k(L)$ for some σ_s.*

TABLE 5.3
Some numerical results of L_b^i/L_b^{i+1}.

i	L_b^i/L_b^{i+1}	i	L_b^i/L_b^{i+1}	i	L_b^i/L_b^{i+1}	i	L_b^i/L_b^{i+1}	i	L_b^i/L_b^{i+1}
1	6.24499800	2	5.45611865	3	5.27609792	4	5.22213335	5	5.20474111
6	5.19900745	7	5.19710323	8	5.19646926	9	5.19625802	10	5.19618762
11	5.19616416	12	5.19615633	13	5.19615373	14	5.19615286	15	5.19615257
16	5.19615247	17	5.19615244	18	5.19615243	19	5.19615242	20	5.19615242

problem, we have

$$\hat{L}_b^i(w) \approx (\frac{\delta\, w}{\sigma_s\,(5\cdot 3^{i-1}-2)})^{1/2}, \tag{5.14}$$

and, since the i-th branch length $L_b^i = w\,3^{1-i}\hat{L}_b^i(w)$, we have

$$\frac{L_b^i}{L_b^{i+1}} \approx 3(\frac{5\cdot 3^i - 2}{5\cdot 3^{i-1}-2})^{1/2} \to 3\sqrt{3}, \quad \text{as } i\to\infty. \tag{5.15}$$

The relation (5.15) and table 5.3 imply that, for laminated microstructures with more than six orders of branches, the branched structure are anisotropically asymptotically self-similar in the sense that the length of the branches decreases by a factor which is increasingly close to $(3\sqrt{3})^{-1}$ while the width of the branches decreases by a factor of 3^{-1}.

Next, we study how the twin width w relies on the total twin length L and the surface energy density σ_s. For needle-like laminates without branch, our numerical experiments show that the characteristic length of the needle $\hat{L}_n$ is usually greater than 20.0. Thus, by (3.24) and (5.8), we see that,

$$w \approx (\frac{2\,L\,\sigma_s}{E_n(\infty,1)})^{1/2} = C_0\,(L\,\sigma_s)^{1/2} \approx 94.4279\,(L\,\sigma_s)^{1/2}, \text{ for } k=0. \tag{5.16}$$

For branched needle-like laminates, by (3.24), (5.9) and (5.14), we have

$$w \approx C(k,\delta)\,L^{2/3}\sigma_s^{1/3}, \text{ for } k \gg 1, \tag{5.17}$$

where

$$C(k,\delta) = (\frac{2}{\sum_{i=1}^k (3^{1-i}\,\delta\,(5-2\cdot 3^{1-i}))^{1/2}})^{2/3} \to C_\infty \approx 3.29311, \quad \text{as } k\to\infty.$$

Our numerical experiments also show that the formula

$$w \approx C\,L^\alpha \sigma_s^{1-\alpha} \tag{5.18}$$

holds for $k=0$ and $k\gg 1$. Table 5 shows some numerical results of the least square data fitting, using the data created by the minimizers of $E^k(L,\cdot)$ (see (3.30)), for the formula (5.18), and it is easily seen that the formula (5.18) holds only in the cases when $k = 0$ or k is sufficiently large so that $\alpha \approx 2/3$ is satisfied. In general, as table 5 suggests, the formula (5.18) might still be true if we consider C as a function of α (for instance we may take $C = C_\infty \exp(C_0(2/3 - \alpha)/4)$ of which the average relative error for the data in table 5 is 5.14%). In any case, numerical evidences show that (5.16) and (5.17) can be taken as a lower and upper bound for the twin width w. Typical numerical results of w as a minimizer of $E^k(L, \cdot)$ for given σ_s are shown in figure 5.7.

TABLE 5.4
Some numerical results of C and α.

σ_s	k, C, α	k, C, α	k, C, α	k, C, α
10^{-6}	0, 91.65, 0.5015	1, 12.92, 0.6108	2, 4.655, 0.6604	3, 2.945, 0.6806
10^{-8}	0, 93.68, 0.5003	1, 34.42, 0.5596	2, 9.795, 0.6215	3, 5.117, 0.6510
10^{-10}	0, 94.14, 0.5001	1, 81.17, 0.5231	2, 35.20, 0.5675	3, 11.96, 0.6155
10^{-8}	4, 3.816, 0.6630	5, 3.370, 0.6675	6, 3.165, 0.6695	7, 3.222, 0.6681
10^{-10}	4, 5.691, 0.6463	5, 4.031, 0.6599	6, 3.567, 0.6644	7, 3.383, 0.6661
10^{-12}	4, 18.05, 0.6057	5, 7.288, 0.6392	6, 4.466, 0.6565	7, 3.661, 0.6634
10^{-10}	8, 3.291, 0.6670	9, 3.262, 0.6672	10, 3.273, 0.6670	11, 3.316, 0.6664
10^{-12}	8, 3.443, 0.6654	9, 3.339, 0.6663	10, 3.311, 0.6666	11, 3.282, 0.6668

In figure 5.7, we can also see that, for fixed k, the length of the first branch L_b^1 is almost a linear function of the total twin laminate length L, and that the needle length L_n grows slightly faster than a linear function of $L^{1/2}$ (in fact it is almost a linear function of L^α as is the growth rate of w). The fact that $L_b^k/L_n \gg 1$, as is shown in figure 5.7, imply that the characteristic lengths of the branches are in general much greater than that of the needles.

6. Summary. The existence of needle-like laminated microstructure with finite order of branches is justified by numerical experiments on a model problem. It is found that, if the surface energy density is sufficiently small and the laminated microstructure is sufficiently long, then the energetically favorable laminated microstructure will have a number of asymptotically self-similar branches. It is also found that smaller surface energy density and longer laminated microstructure imply greater number of branches. The theory and the numerical experiments show that the twin width is proportional to $L^{1/2}\sigma_s^{1/2}$ if the laminated microstructure has no branch, and it is proportional to $L^{2/3}\sigma_s^{1/3}$ if the laminated microstructure has great number of branches. The numerical experiments also show that the distance from the very first branch to the austenite-finely twined martensite interface is in general no greater than one third of the total twin laminate length.

Acknowledgement: The author wish to thank the referees for their valuable suggestions and comments.

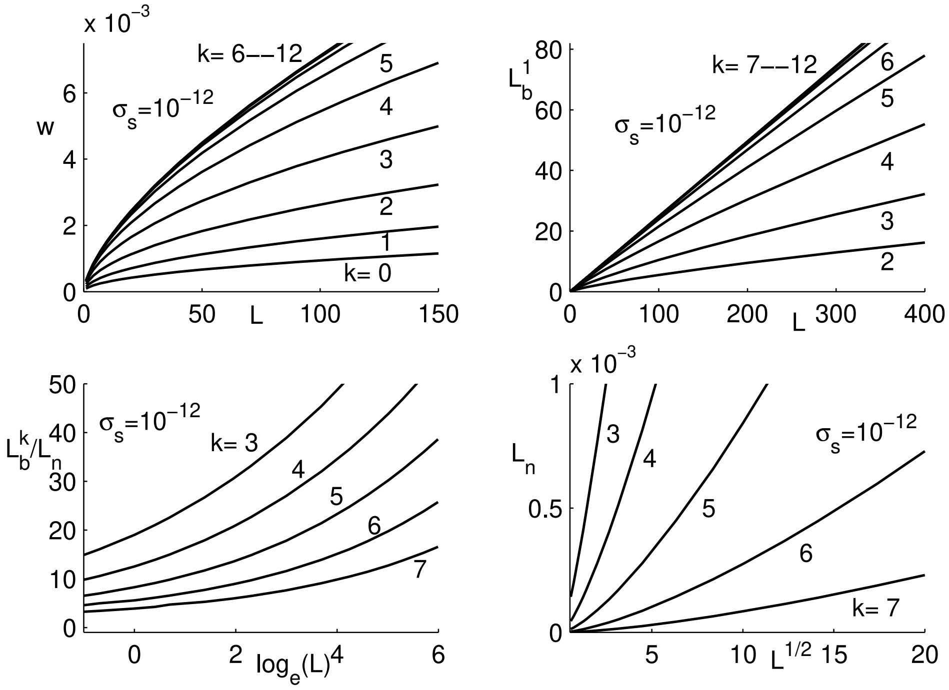

FIG. 5.7. *w, L_b^1, L_b^k/L_n and L_n as functions of L.*

REFERENCES

[1] J. M. Ball and R. D. James, *Fine phase mixtures as minimizers of energy.* **Arch. Rat. Mech. Anal., 100**(1987)1, 13-52.

[2] J. M. Ball and R. D. James, *Proposed experimental test of a theory of fine microstructure and the two-well problem.* **Phil. Trans. R. Soc. London 338A**(1992), 389-450.

[3] M. Chipot and D. Kinderlehrer, *Equilibrium configurations of crystals*, **Arch. Rat. Mech. Anal., 103**(1988)1, 237-277.

[4] D. Kinderlehrer, *Remarks about equilibrium configurations of crystals*, in **Material Instabilities in Continuum Mechanics and Related Problems**, J. M. Ball, ed., Oxford University press, 1987, pp. 217-242.

[5] R.V. Kohn and Stefan Müller, *Branching of twins near an austenite-twinned-martensite interface.* **Phil. Mag., A 66**(1992), 697-715.

[6] R.V. Kohn and Stefan Müller, *Surface energy and microstructure in coherent phase transitions.* **Comm. Pure Appl. Math., 47**(1994), 405-435.

[7] S. Conti, *Branched microstructures: scaling and asymptotic self-similarity.* **Comm. Pure Appl. Math., 53**(2000), 1448-1474.

[8] L. Truskinovsky and G. Zanzotto, *Ericksen's bar revisited: enrgy wiggles.* **J. Mech. Phys. Solids, 44**(8)(1996), 1371-1408.

[9] X. Ren and L. Truskinovsky, *Finite scale microstructures in nonlocal elasticity.* **J. Elasticity 59**(2000), 319-355.

[10] B. Li and M. Luskin, *Theory and computation for the microstructure near the interface between twinned layers and a pure variant of martensite.* **Materials Sci. Eng. A-Struct. 275** (1999), pp. 237-240.

[11] M. Chipot and Stefan Müller, *Sharp energy estimates for finite element approximations of non-convex problems.* In: **Variations of domain and free-boundary problems in solid mechanics** (Paris). Kluwer (1997), pp.317-325.

[12] S. Bartels and A. Prohl, *Multiscale solution in the computation crystalline microstructure.* preprint.

[13] Z.-P. Li, *Rotational transformation method and some numerical techniques for the computation of microstructures.* **Math. Models Meth. Appl. Sci., 8**(1998), 985-1002.

[14] Z.-P. Li, *A periodic relaxation method for computing microstructures.* **Appl. Numer. Math., 32**(2000), 291-303.

[15] Z.-P. Li, *Computations of needle-like microstructures*, **Appl. Numer. Math., 39**(2001), 1-15.

[16] Z.-P. Li, *Mesh transformation and regularization in numerical simulation of austenitic-martensitic phase transition.* **Comp. Material Sci., 21**(2001), 418-428.

[17] Z.-P. Li, *A mesh transformation method for computing microstructures.* **Numer. Math., 89**(2001), 511-533.

[18] Z. -P. Li, *A numerical study on the scale of laminated microstructure with surface energy.* To appear in **Materials Sci. Eng. A**.

[19] C. Collins, *Computation of twinning*, in **Microstructure and Phase Transitions**, IMA Volumes in Mathematics and Its Applications, Vol.54, J. Ericksen, R. James, D. Kinderlehrer and M. Luskin, eds, Springer-Verlag, New York, (1993), pp. 39-50.

[20] C. Collins, M. Luskin and J. Riordan, *Computational results for a two-dimensional model of crystalline microstructure*, in **Microstructure and Phase Transitions**, IMA Volumes in Mathematics and Its Applications, Vol.54, J. Ericksen, R. James, D. Kinderlehrer and M. Luskin, eds, Springer-Verlag, New York, (1993), pp. 51-56.

[21] M. Luskin, *On the computation of crystalline microstructure.* **Acta Numerica, 5**(1996), 191-257.

[22] Z.-P. Li, *Laminated microstructure in a variational problem with a non-rank-one connected double well potential*, **J. Math. Anal. Appl., 217**(1998), 490-500.

[23] C. Collins and M Luskin, *The computation of the austenitic-martensitic phase transition.* In **Partial Differential Equations and Continuum Models of Phase Transitions** Lecture Nodes in Physics, Vol. 344, M. Rascle, D. Serre and M. Slemrod, eds, Springer-Verlag, New York, (1989), pp. 34-50.

[24] P. Klouček and M. Luskin, *The computation of the dynamics of the martensitic transformation*, *Continuum Mech. Thermodyn., 6*(1994), 209-240.

[25] P. G. Ciarlet, **Mathematical Elasticity**, Volume 1: Three Dimensional Elasticity. North-Holland, Amsterdam, 1988.

[26] P.G. Ciarlet, **The Finite Element Method for Elliptic Problems**. North-Holland, Amsterdam, 1978.